A many-body approach to spin-wave excitations in itinerant magnetic systems

2000 J. Phys.: Condens. Matter 12 7617

(http://iopscience.iop.org/0953-8984/12/34/308)

J. Phys.: Condens. Matter **12** (2000) 7617–7631. Printed in the UK PII: S0953-8984(00)14284-5

A many-body approach to spin-wave excitations in itinerant magnetic systems

K Karlsson† and F Aryasetiawan‡

† Institutionen för Naturvetenskap, Högskolan i Skövde, 54128 Skövde, Sweden
‡ Joint Research Centre for Atom Technology—Angstrom Technology Partnership, 1-1-4 Higashi, Tsukuba, Ibaraki 305, Japan

Received 24 May 2000, in final form 20 July 2000

Abstract. Using a recently developed Green's function formalism, we have calculated the spin-wave spectra and dispersions in Ni and Fe. For Ni(100), the dispersion exhibits two branches as observed experimentally. The calculated higher optical branch is found to be too high in energy when the standard local density approximation band-structure is used but a very good agreement with the measured dispersion is obtained when the exchange splitting is reduced, to correspond to the experimental value of the exchange splitting. We also found a double branch along Ni(111) which is not observed experimentally. For Fe, the calculated dispersion surprisingly exposes a gap midway along Γ–N in disagreement with experimental data. However, an analysis of the temperature-dependent magnetization has predicted a similar gap at the same wave vector, supporting the present calculations.

1. Introduction

In a previous work [1] (hereafter referred to as paper I) we developed a formalism for calculating spin-wave spectra based on the Green function method. The formalism does not rely on any assumption about the spin nature of the electrons being itinerant or localized. This is in contrast to the common frozen-magnon procedure which usually maps the spin-wave problem to the Heisenberg Hamiltonian with the assumption of localized spins [2–6]. In the simplest approximation, the formalism proposed in the previous work reduces to the well-known random-phase approximation (RPA) [7–11]. The method, however, is rather general. The interactions among the electrons naturally turned out to be nonlocal. Another advantage of the formalism is that it gives not only the spin-wave dispersions but also the spectra as functions of wave vectors and frequencies. This allows the determination of spin-wave lifetimes as well as multiple branches which it is not possible to obtain within the frozen-magnon approach.

Spin-wave spectra can also be calculated using time-dependent density functional theory (TD DFT). The most recent calculation using this method was performed by Savrasov [12] for Fe, Ni, and Cr. Although the method is formally exact, the calculated spectra may depend significantly on the quality of the exchange–correlation potential. Our formalism shows that the interactions among the electrons can be very nonlocal and such a nonlocality can be difficult to take into account using a constant exchange–correlation kernel derived from the local density approximation (LDA). In electronic structure calculations, the major part of the effective one-particle potential is the Hartree potential and a relatively crude approximation for the exchange–correlation potential, such as that of the LDA, is sufficient in many cases. In calculating spin-wave spectra on the other hand, it is the derivative of the exchange–correlation

0953-8984/00/347617+15$30.00

potential with respect to the density which is the main ingredient. Thus, a simple approximation may not be adequate and not surprisingly, the spin-wave dispersions calculated within the LDA using the frozen-magnon approach often show a large discrepancy with experiment.

In the present work, we apply our formalism to the classical examples of spin waves in Ni and Fe which have been studied by a number of authors using different approaches. These systems provide a stringent test for the applicability of the formalism. The experimental spin-wave dispersion of Ni [13] shows a number of interesting features which have not been fully explained. A prominent feature is the presence of two branches, known as the 'acoustic' and 'optical' branches. Early and more current studies did succeed in reproducing the two branches but there are some problems [9, 12, 14]. In earlier calculations, for some wave vectors, the intensity of the acoustic branch is higher than that for the optical branch, whereas experimentally it is the other way round [14]. More recent and probably the most up-to-date calculation using TD DFT gives a dispersion showing significant deviation from experiment for the optical branch [12]. A possible explanation is that the exchange–correlation kernel derived from the LDA is not adequate to describe the interactions among the spins. Another possibility is that the Kohn–Sham band-structure is substantially in error as compared with the photoemission (quasiparticle) band-structure. In particular, the exchange splitting, which is relevant for determining the spin-wave dispersion, is overestimated by the LDA by a factor of two [15]. The origin of the discrepancy in the optical branch is investigated in the present work.

For Fe, existing calculations [9, 12, 16–19] have been successful in reproducing the experimental dispersion [20, 21], at least for small momentum transfer. However, a very interesting analysis of the temperature-dependent magnetization of Fe predicts a gap in the spin-wave dispersion at about 0.74 Å^{-1} which is necessary to explain the experimental magnetization data [22]. Such a crossover gap between the acoustic and optical branches is in fact not observed experimentally since the accuracy of the experimental data is often limited by experimental broadening, background contributions, and random noise. Numerical calculations on the other hand can be performed with a rather high accuracy which allows us to observe features which may not be easily seen experimentally. As will be shown later, our calculations also predict a gap at almost exactly the same wave vector as predicted by Ododo and Anyakoha [22].

Another unsettled issue common to Ni and Fe is that of whether the dispersion extends to the zone boundaries (ZB). Experimentally, the signal from neutron scattering is diminishing as one approaches the ZB. This is particularly the case for the lower acoustic branch in Ni. On the other hand, neutron scattering investigation of Fe [21] predicts the magnon to exist out to the ZB. However, no information about the intensity was given and the effects of the experimental resolution were not properly taken into account. Previous numerical calculations, however, predicted the existence of spin-wave excitations right to the ZB. This issue is also investigated in the present work.

2. Theory

2.1. Basic relations

Spin excitation spectra can be measured by inelastic neutron scattering experiments. The neutron scattering cross section can be directly related to the imaginary part of the magnetic response function (see the appendix). The spin-wave excitation spectrum is given by the following spectral function:

$$S^{-+}(\boldsymbol{r}, \boldsymbol{r}', \omega) \equiv Z^{-1} \sum_{jk} \mathrm{e}^{-\beta(E_j - \mu N)}(1 - \mathrm{e}^{-\beta\omega})\langle j|\hat{\sigma}^-(\boldsymbol{r})|k\rangle\langle k|\hat{\sigma}^+(\boldsymbol{r}')|j\rangle\delta(\omega - E_k + E_j). \tag{1}$$

The physical meaning of $\hat{\sigma}^+(\boldsymbol{r})$ is that it increases the spin of an electron at $\boldsymbol{r}$ by one. The spin of the states $|k\rangle$ must therefore be larger by one than that of the states $|j\rangle$, i.e. the states $|k\rangle$ contain a spin-wave excitation. Thus, a peak in S^{-+} may be identified with a spin-wave excitation. The quantity R^{-+} is related to the response functions.

First we briefly sketch some ideas discussed in paper I. The charge and magnetic τ-ordered response function is defined by

$$\mathcal{R}_{ij}(1,2) \equiv \frac{\delta\langle\hat{\sigma}^i(1)\rangle}{\delta\varphi_j(2)} \tag{2}$$

where $i, j = 0, x, y, z$. The external field φ_j corresponds to a scalar one for $j = 0$ and to the magnetic field for $j = x, y, z$. Here, $1 \equiv (\boldsymbol{r}, \tau)$; α and β denote the spin. The spin density is given by

$$\langle\hat{\sigma}^i(1)\rangle = \sigma^i_{\beta\alpha}\mathcal{G}_{\alpha\beta}(1, 1^+) \tag{3}$$

where a repeated index or variable implies a summation or integration provided that the index or variable does not appear on the other side of the equation. $\mathcal{G}_{\alpha\beta}$ is the Matsubara (temperature) Green function. The Pauli spin matrices are given by

$$\sigma^0 = \begin{pmatrix} 1 & 0 \\ 0 & 1 \end{pmatrix} \qquad \sigma^x = \begin{pmatrix} 0 & 1 \\ 1 & 0 \end{pmatrix} \qquad \sigma^y = \begin{pmatrix} 0 & -\mathrm{i} \\ \mathrm{i} & 0 \end{pmatrix} \qquad \sigma^z = \begin{pmatrix} 1 & 0 \\ 0 & -1 \end{pmatrix}. \tag{4}$$

The exact expression for the response function reads

$$\mathcal{R}_{ij}(1,2) = \sigma^i_{\beta\alpha}\mathcal{G}_{\alpha\mu}(1,4)\left[\delta(4-5)\epsilon^{-1}_{j,\mu\nu}(4,2) + \frac{\delta\Sigma_{\mu\nu}(4,5)}{\delta\varphi_j(2)}\right]\mathcal{G}_{\nu\beta}(5,1^+) \tag{5}$$

where we have defined

$$\epsilon^{-1}_{j,\alpha\beta}(1,2) \equiv \left[\sigma^j_{\alpha\beta}\delta(1-2) + \sigma^0_{\alpha\beta}\frac{\delta V_H(1)}{\delta\varphi_j(2)}\right]. \tag{6}$$

Here V_H denotes the Hartree potential and Σ the electron self-energy. Naturally, without $\delta\Sigma/\delta\varphi$ there will be no magnetic response since the response function reduces to that of the time-dependent Hartree approximation.

Diagrammatically, the response function consists of a closed electron–hole diagram (bubble) with a spin-flip centre at one end and an electron–hole diagram with the nonlocal vertex $\delta\Sigma/\delta\varphi$ inserted. We now take into account the vertex with the self-energy within the GWA [23] and only consider the change in $\mathcal{G}$. It is necessary to allow the Green function to have nondiagonal components in spin space, for otherwise there would be no spin fluctuations in the xy-directions. Thus

$$\begin{aligned}\frac{\delta\Sigma_{\alpha\beta}(1,2)}{\delta\varphi_j(3)} &= -\frac{\delta\mathcal{G}_{\alpha\beta}(1,2)}{\delta\varphi_j(3)}\mathcal{W}(1,2) \\ &= -\mathcal{W}(1,2)\mathcal{G}_{\alpha\mu}(1,4)\left\{\epsilon^{-1}_{j,\mu\nu}(4,3)\mathcal{G}_{\nu\beta}(4,2) + \frac{\delta\Sigma_{\mu\nu}(4,5)}{\delta\varphi_j(3)}\mathcal{G}_{\nu\beta}(5,2)\right\}.\end{aligned} \tag{7}$$

This is an integral equation for the vertex which can be solved formally as follows:

$$\begin{aligned}&\left\{\delta_{\mu\alpha}\delta_{\nu\beta}\delta(4-1)\delta(5-2) + \mathcal{W}(1,2)\mathcal{G}_{\alpha\mu}(1,4)\mathcal{G}_{\nu\beta}(5,2)\right\}\frac{\delta\Sigma_{\mu\nu}(4,5)}{\delta\varphi_j(3)} \\ &\quad = -\mathcal{W}(1,2)\mathcal{G}_{\alpha\mu}(1,4)\epsilon^{-1}_{j,\mu\nu}(4,3)\mathcal{G}_{\nu\beta}(4,2).\end{aligned} \tag{8}$$

Defining

$$\mathcal{D}_{\alpha\beta,\mu\nu}(1,2|3,4) \equiv \delta_{\mu\alpha}\delta_{\nu\beta}\delta(3-1)\delta(4-2) + \mathcal{W}(1,2)\mathcal{G}_{\alpha\mu}(1,3)\mathcal{G}_{\nu\beta}(4,2) \tag{9}$$

$$\Pi_{j,\alpha\beta}(1,2|3) \equiv \mathcal{G}_{\alpha\mu}(1,4)\epsilon^{-1}_{j,\mu\nu}(4,3)\mathcal{G}_{\nu\beta}(4,2) \tag{10}$$

$$\mathcal{N}_{j,\alpha\beta}(1,2|3) \equiv -\mathcal{W}(1,2)\Pi_{j,\alpha\beta}(1,2|3) \tag{11}$$

the vertex is given by (shown diagrammatically in figure 1)

$$\Lambda_{j,\alpha\beta}(1,2|3) \equiv \frac{\delta\Sigma_{\alpha\beta}(1,2)}{\delta\varphi_j(3)} = \mathcal{D}^{-1}_{\alpha\beta,\mu\nu}(1,2|4,5)\mathcal{N}_{j,\mu\nu}(4,5|3). \tag{12}$$

When substituted into equation (5), this vertex correction results in ladder diagrams. In fact, the resulting response function is equivalent to the well-known RPA magnetic response function.

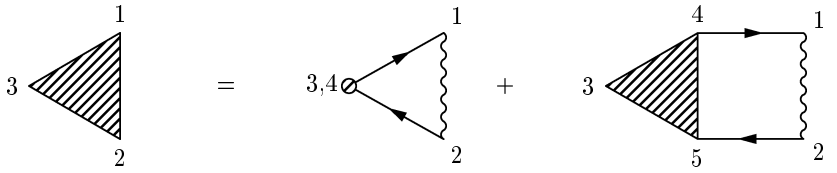

Figure 1. Feynman diagrams for the vertex in equation (7). The solid line represents the Green function, the wiggly line the screened interaction $\mathcal{W}$, and the small circle ϵ^{-1}_j.

2.2. Local approximation

Recent TD DFT calculations [12] show significant deviation from experiment, especially for Ni, and it was argued that the main source of the problem is the local and static nature of the exchange–correlation functional. On the other hand, the results for Fe are in good agreement with experiment. We know that the band-structure of Ni in the LDA suffers from a few problems. Relevant to our calculations is the fact that the exchange splitting is overestimated by a factor of two whereas this is not the case for Fe. It is likely that it is the error in the exchange splitting in Ni that is responsible for the poor agreement for the optical branch in the spin-wave dispersion. In order to investigate this problem we will solve for the response function (equation (5)) using a *local* and *static* screened interaction $\mathcal{W}$.

If we transform the vertex equation into Fourier space using a static screened potential, it becomes

$$\left[\delta(1-4)\delta(2-5) - \mathcal{W}(1,2)\mathcal{K}^{\alpha\beta}(12,45;\omega_m)\right]\Lambda_{j,\alpha\beta}(4,5,3;\omega_m) = \frac{1}{\beta}\mathcal{W}(1,2)\sigma^j_{\alpha\beta}\mathcal{K}^{\alpha\beta}(12,33;\omega_m) \tag{13}$$

and where we assume that the Green function is now diagonal in spin space. ν_m denotes a Matsubara frequency for fermion propagators and for bosons we use ω_n as a convention. Hereafter $1 \equiv \boldsymbol{r}_1$.

We also introduce the kernel $\mathcal{K}$ as

$$\mathcal{K}^{\alpha\beta}(12,45;\omega_m) = -\frac{1}{\beta}\mathcal{G}_\alpha(1,4;\omega_m+\nu_k)\mathcal{G}_\beta(5,2;\nu_k). \tag{14}$$

Using a noninteracting Green function:

$$\mathcal{G}_\alpha(1,2;\nu_m) = \frac{\psi_{\boldsymbol{k}n\alpha}(1)\psi^*_{\boldsymbol{k}n\alpha}(2)}{\mathrm{i}\nu_m - \varepsilon_{\boldsymbol{k}n\alpha}} \tag{15}$$

the summation over frequencies in the kernel can be performed analytically (see e.g. p 272 of reference [24]), giving

$$\mathcal{K}^{\alpha\beta}(12,45;\omega_m) = \psi_{\boldsymbol{k}n\alpha}(1)\psi^*_{\boldsymbol{k}'n'\beta}(2)\psi^*_{\boldsymbol{k}n\alpha}(4)\psi_{\boldsymbol{k}'n'\beta}(5)\frac{f(\varepsilon_{\boldsymbol{k}n\alpha}) - f(\varepsilon_{\boldsymbol{k}'n'\beta})}{\mathrm{i}\omega_m + \varepsilon_{\boldsymbol{k}'n'\beta} - \varepsilon_{\boldsymbol{k}n\alpha}}. \tag{16}$$

Here $\{\psi_{kn}, \epsilon_{kn}\}$ are the LDA Bloch states and the corresponding eigenvalues, respectively. If we now use the local approximation and for simplicity assume zero temperature, the kernel becomes

$$\mathcal{K}^{\alpha\beta}(11, 44; \omega_m) = \sum_{\boldsymbol{k}\boldsymbol{k}'} \sum_{n}^{occ} \sum_{n'}^{unocc} \frac{\psi_{\boldsymbol{k}n\alpha}(1)\psi^*_{\boldsymbol{k}'n'\beta}(1)\psi_{\boldsymbol{k}'n'\beta}(4)\psi^*_{\boldsymbol{k}n\alpha}(4)}{(\mathrm{i}\omega_m + \epsilon_{\boldsymbol{k}'n'\beta} - \epsilon_{\boldsymbol{k}n\alpha})} - \frac{\psi_{\boldsymbol{k}n\beta}(1)\psi^*_{\boldsymbol{k}'n'\alpha}(1)\psi_{\boldsymbol{k}'n'\alpha}(4)\psi^*_{\boldsymbol{k}n\beta}(4)}{(\mathrm{i}\omega_m - \epsilon_{\boldsymbol{k}'n'\alpha} + \epsilon_{\boldsymbol{k}n\beta})}. \tag{17}$$

The kernel is continued analytically to real frequencies $\omega_n \to \omega + \mathrm{i}\delta$. Finally we define $\mathcal{S}$ as follows:

$$\mathcal{S}^{\alpha\beta}(1, 2; \omega) = \sum_{\boldsymbol{k}\boldsymbol{k}'} \sum_{n}^{\mathrm{occ}} \sum_{n'}^{\mathrm{unocc}} \psi_{\boldsymbol{k}n\alpha}(1)\psi^*_{\boldsymbol{k}'n'\beta}(1)\psi_{\boldsymbol{k}'n'\beta}(2)\psi^*_{\boldsymbol{k}n\alpha}(2)\delta(\omega + \epsilon_{\boldsymbol{k}'n'\beta} - \epsilon_{\boldsymbol{k}n\alpha}) - \psi_{\boldsymbol{k}n\beta}(1)\psi^*_{\boldsymbol{k}'n'\alpha}(1)\psi_{\boldsymbol{k}'n'\alpha}(2)\psi^*_{\boldsymbol{k}n\beta}(2)\delta(\omega - \epsilon_{\boldsymbol{k}'n'\alpha} + \epsilon_{\boldsymbol{k}n\beta}). \tag{18}$$

Since $\mathcal{S}$ is real we can write

$$\mathcal{K}^{\alpha\beta}(1, 2; \omega) = \int \mathrm{d}\omega' \, \frac{\mathcal{S}^{\alpha\beta}(1, 2; \omega')}{\omega - \omega' + \mathrm{i}\delta} \tag{19}$$

so $\mathrm{Im}\,\mathcal{K}$ is directly related to $\mathcal{S}$. The main task is to calculate $\mathcal{S}$ and then the real part of the kernel is obtained as the principal part, i.e.

$$\mathrm{Re}\,\mathcal{K}^{\alpha\beta}(1, 2; \omega) = \mathcal{P} \int \mathrm{d}\omega' \, \frac{\mathcal{S}^{\alpha\beta}(1, 2; \omega')}{\omega - \omega'}. \tag{20}$$

For practical calculations, it is suitable to use Bloch basis functions $B_{\boldsymbol{q}r}$ for the space variables [25]. Using the static and local potential for the screened potential $\mathcal{W}$ we get for the vertex equation

$$\left[\delta_{rp} - \mathcal{W}_{rt}\mathcal{K}^{\alpha\beta}_{tp}(\boldsymbol{q}, \omega)\right] \Lambda^{ps}_{j,\alpha\beta}(\boldsymbol{q}; \omega) = \mathcal{W}_{rt}\mathcal{K}^{\alpha\beta}_{ts}(\boldsymbol{q}, \omega) \tag{21}$$

where

$$\begin{aligned} \mathcal{W}_{rs} &= \langle B_{\boldsymbol{q}r}|\mathcal{W}(\boldsymbol{r}, \boldsymbol{r}' = \boldsymbol{r}; \omega = 0)|B_{\boldsymbol{q}s}\rangle \\ \mathcal{K}^{\alpha\beta}_{rs}(\boldsymbol{q}, \omega) &= \langle B_{\boldsymbol{q}r}|\mathcal{K}^{\alpha\beta}(\boldsymbol{r}, \boldsymbol{r}'; \omega)|B_{\boldsymbol{q}s}\rangle \\ \Lambda^{rs}_{j,\alpha\beta}(\boldsymbol{q}; \omega) &= \langle B_{\boldsymbol{q}r}|\Lambda_{j,\alpha\beta}(\boldsymbol{r}, \boldsymbol{r}'; \omega)|B_{\boldsymbol{q}s}\rangle. \end{aligned} \tag{22}$$

The $\boldsymbol{q}$-component of the response function is obtained by taking the matrix element

$$\begin{aligned} \mathcal{R}_{ij}(\boldsymbol{q}, \omega) &= \int \mathrm{d}^3r \, \mathrm{d}^3r' \exp(-\mathrm{i}\boldsymbol{q}\cdot\boldsymbol{r})\mathcal{R}_{ij}(\boldsymbol{r}, \boldsymbol{r}'; \omega)\exp(\mathrm{i}\boldsymbol{q}\cdot\boldsymbol{r}') \\ &= -\sigma^i_{\beta\alpha}\sigma^j_{\alpha\beta}\langle \boldsymbol{q}|B_{\boldsymbol{q}r}\rangle \left[\mathcal{K}^{\alpha\beta}_{rs}(\boldsymbol{q}, \omega) + \mathcal{T}^{\alpha\beta}_{rs}(\boldsymbol{q}, \omega)\right] \langle B_{\boldsymbol{q}s}|\boldsymbol{q}\rangle \end{aligned} \tag{23}$$

where

$$\langle \boldsymbol{q}|B_{\boldsymbol{q}r}\rangle = \int \mathrm{d}^3r \, \exp(-\mathrm{i}\boldsymbol{q}\cdot\boldsymbol{r})B_{\boldsymbol{q}r}(\boldsymbol{r}) \tag{24}$$

and schematically

$$\mathcal{T} = \mathcal{K}\Lambda = \mathcal{K}[1 - \mathcal{W}K]^{-1}\mathcal{W}\mathcal{K}. \tag{25}$$

We have developed a scheme using a localized product basis [25], based on the linear muffin-tin orbital (LMTO) method within the atomic sphere approximation [26]. The number of basis functions used is 40 per atom. The number of $\boldsymbol{k}$-points in the entire zone is more than 40 000,

which corresponds to 1000 points in the irreducible zone. The delta function in the imaginary part of kernel is replaced by a Gaussian

$$(\sqrt{\pi}\sigma)^{-1}\exp(-\omega^2/\sigma^2). \tag{26}$$

We have used this technique rather than the tetrahedron method because we wish to investigate the effects of broadening on the spectra.

The spin-wave spectrum is given by $\operatorname{Im}\mathcal{R}_{-+}(\boldsymbol{q},\omega) \sim \operatorname{Im}\mathcal{R}_{xx}(\boldsymbol{q},\omega)$ and the spin-wave excitation energy ω_q can be identified with the position of the main peak in $\operatorname{Im}\mathcal{R}_{-+}(\boldsymbol{q},\omega)$ (see appendix A).

3. Results and discussion

3.1. Ni(100)

The experimental dispersion of Ni along (1 0 0) exhibits two branches between about (0.2 0 0) and (0.6 0 0) [13]. The experimental dispersion ends at (0.6 0 0) due the broadening of the spin-wave excitation peak as it approaches the ZB as indicated by the large error bar. The large broadening makes it difficult to detect the presence of spin-wave excitations. The dispersion for small q shows the expected quadratic behaviour for ferromagnetic systems.

The dispersion has been calculated before by a number of authors [9, 10, 14]. The most recent calculation [12] using TD DFT is capable of reproducing the acoustic branch quite well but the calculated optical branch shows a large discrepancy with experiment. TD DFT formally can give the exact spin-wave excitation spectra provided that one has the exact time-dependent exchange–correlation potential. In practice, however, the calculations are performed within the adiabatic LDA and the generalized gradient approximation (GGA) [27] leading to possible errors. The local nature of the exchange–correlation kernel and possible errors in the Kohn–Sham eigenvalues are the two main consequences of an approximate exchange–correlation potential.

In an ordinary LDA calculation for Ni the exchange splitting for states at the top of the occupied band is overestimated by a factor of two compared to experiment (0.3 eV versus 0.6 eV) [15]. The discrepancy is mainly due to self-energy effects, not properly taken into account in the LDA. Consequently, a Stoner spin-flip process (described by $\mathcal{S}^{\alpha\beta}$ with $\alpha \neq \beta$) costs too much in energy when using the LDA eigenvalues. To investigate the role of the one-particle band-structure we first calculate the spin-wave spectra using the ordinary LDA band-structure. The results are similar to those of Savrasov [12, 28] as expected. In agreement with experiment [13], the spin-wave dispersion curve exhibits two branches. However, as already mentioned, the energy of the optical spin-wave mode is much too large. This was suggested to be due to a poor treatment of the dynamical exchange correlation in the GGA, which has the same problem as the local and static exchange correlation kernel within the LDA.

According to experiment and a recent calculation [29], the exchange splitting of Ni should be one half of that of the LDA. We therefore decrease the exchange splitting by one half, which has the consequence of reducing the energy for a Stoner spin-flip process also by a factor of one half. The corresponding spin-wave dispersion curve is shown in figure 2. A drastic reduction in the energy of the optical spin-wave branch is found, leading to a very good agreement with the experiment of Mook and Paul [13]. The existence of two spin-wave branches is still maintained but the optical mode is lowered and it coincides with the experimental curve. The main difference between the calculated dispersion and the experiment is that the calculated low-energy acoustic branch is disappearing for slightly smaller $\boldsymbol{q}$-values. The reason for this could be related to the use of broadening in our calculations which smears out the possible presence of a two-peak structure in the spectra.

It is interesting to note that the spin-wave excitation energy ω_q is merely constant for $\boldsymbol{q} > 0.6(1, 0, 0)2\pi/a$. The present result strongly indicates that the main source of problems in the TD DFT calculation can be traced back to the wrong LDA eigenvalues for Ni, in particular the exchange splitting. This is also supported by the fact that for Fe, where the LDA eigenvalues are in agreement with photoemission data, no reduction in the exchange splitting is necessary as shown later. Moreover, the TD DFT results are also in good agreement with experiment.

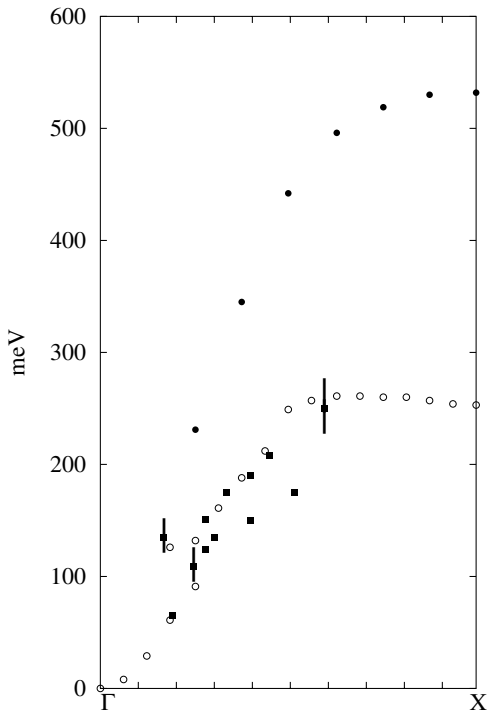

Figure 2. Spin-wave dispersion along (100) for nickel. Black boxes corresponds to the experiment by Mook and Paul. Error bars are indicated by vertical solid lines. Also shown (black circles) are the optical modes resulting from calculations by Savrasov [12]. The empty circles correspond to the present calculations. The Gaussian broadening σ in equation (26) is 0.02 eV.

We now discuss the origin of the two branches. From the equation for the response function, a double-peak structure in the spin-wave spectra may arise either from a complicated band-structure implicitly contained in the kernel $\mathcal{K}$ or from a strong energy dependence in $\mathcal{W}$. Our results suggest that it is mainly the band-structure that is responsible for the presence of the two branches since we have used a static $\mathcal{W}$ in the calculations. Typically, $\mathrm{Im}\,\mathcal{K}$ is peaked at about the average exchange-splitting energy corresponding to the Stoner spin-flip excitation where an electron from the majority channel is excited into the minority channel. Due to correlations, $1 - \mathcal{W}\,\mathrm{Re}\,\mathcal{K}$ and $\mathrm{Im}\,\mathcal{K}$ can both become zero or small at an energy below the Stoner peak. This gives rise to a collective excitation or spin waves. Generally speaking, the appearance of more than one spin-wave excitation, like the double-peak structure in the spin-wave spectra of Ni, implies the presence of additional structure in $\mathrm{Im}\,\mathcal{K}$ below the Stoner peak.

In figures 3 and 4 we show a typical matrix element for $1 - \mathcal{W}\,\mathrm{Re}\,\mathcal{K}$ and $\mathrm{Im}\,\mathcal{K}$ for the case where we used a band-structure with a reduced exchange splitting. Not displayed are the Stoner peaks located at approximately 0.3 eV. Additional structures below the Stoner peak are

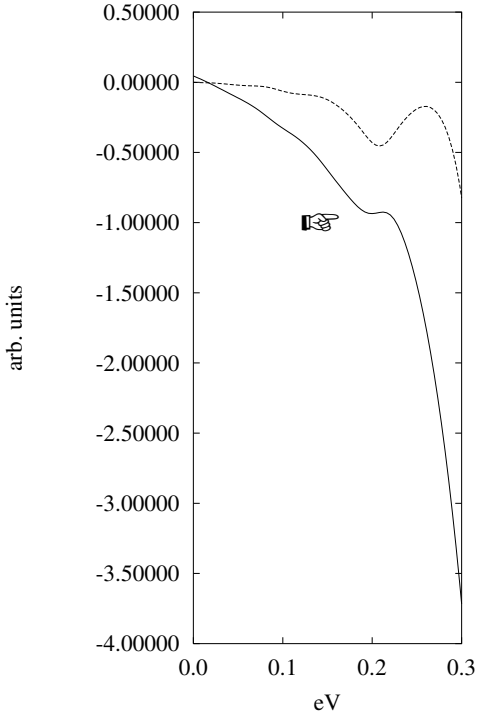

Figure 3. The $i = j = 1$ matrix element of $1 - \mathcal{W}\,\mathrm{Re}\,\mathcal{K}$ (solid line) and that of $\mathcal{W}\,\mathrm{Im}\,\mathcal{K}$ (dashed line) for nickel; $\boldsymbol{q} = 0.0625(1, 0, 0)2\pi/a$. The structure pointed at by a small hand is explained in the text.

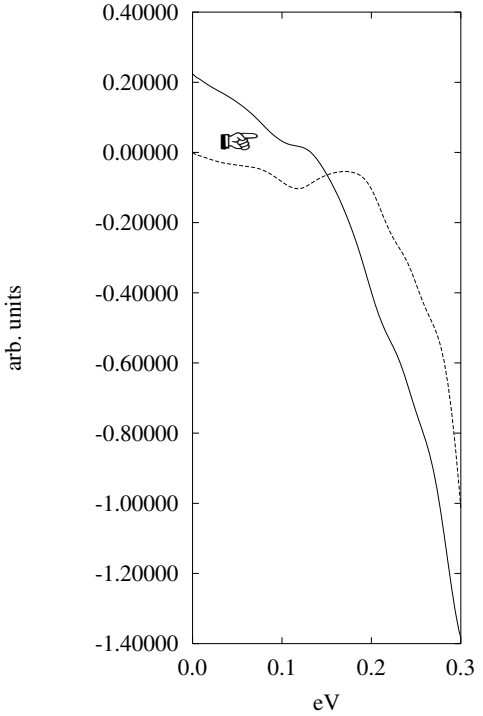

Figure 4. The $i = j = 1$ matrix element of $1 - \mathcal{W}\,\mathrm{Re}\,\mathcal{K}$ (solid line) and that of $\mathcal{W}\,\mathrm{Im}\,\mathcal{K}$ (dashed line) for nickel; $\boldsymbol{q} = 0.25(1, 0, 0)2\pi/a$. The structure pointed at by a small hand is explained in the text.

clearly visible; these give rise to the double-peak structure leading to the two branches in the dispersion.

The double peak is most distinctly observed for $\boldsymbol{q} = 0.25(1, 0, 0)2\pi/a$ in figure 5. Due to a large density of states around the Fermi level which is mainly of 3d character, d–d transitions (hopping from the occupied majority-spin to the unoccupied minority-spin channel) are enhanced and result in the small peak around 0.1 eV in $\mathcal{W}\,\mathrm{Im}\,\mathcal{K}$. This in turn gives rise to a weak dip structure in $1 - \mathcal{W}\,\mathrm{Re}\,\mathcal{K}$ via the Kramers–Kronig relation. For $\boldsymbol{q} \sim (0.15\text{–}0.3, 0, 0)2\pi/a$ the dip structure in $1 - \mathcal{W}\,\mathrm{Re}\,\mathcal{K}$ is located close to zero and consequently there will be *two peaks* in the spin-wave excitation spectra. The presence of the double-peak structure is rather sensitive to both the position and intensity of the smaller peak. Thus for smaller and larger $\boldsymbol{q}$-values the dip structure does not give rise to any poles in $(1 - \mathcal{W}\,\mathrm{Re}\,\mathcal{K})^{-1}$ as illustrated in figure 3. For large $\boldsymbol{q}$, it is actually the position of the main peak in $\mathcal{W}\,\mathrm{Im}\,\mathcal{K}$ that determines the spin-wave spectra.

The lower acoustic branch does not extend to the zone boundary, as also found experimentally. The physical interpretation is that the spin-wave excitations merge with the Stoner excitations as the former approaches the zone boundary with increasing wave vector. The Stoner excitations exist in principle at all energies but the main excitations are centred around the average exchange-splitting energy. The linewidth of the spin-wave excitations is determined by $\mathrm{Im}\,\mathcal{K}$ which increases with energy to form the Stoner peak. As the wave vector increases, the spin-wave energies at which $\mathcal{W}\,\mathrm{Im}\,\mathcal{K}$ and $1 - \mathcal{W}\,\mathrm{Re}\,\mathcal{K}$ are zero or small also increase, so the linewidth increases accordingly.

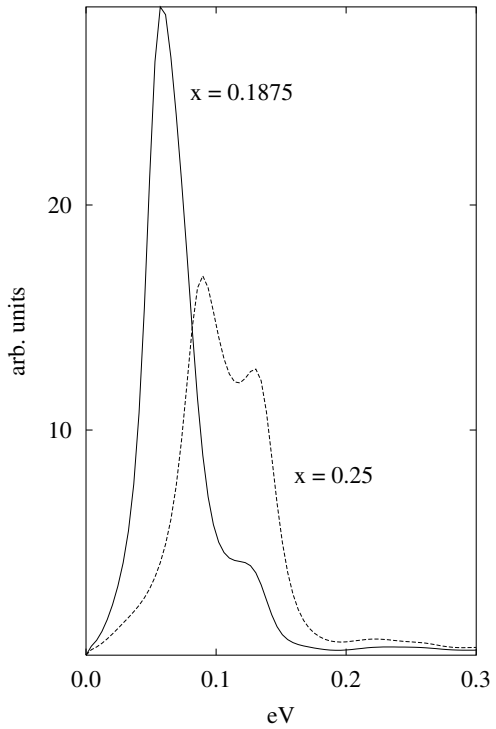

Figure 5. Spin-wave excitation spectra of nickel for $\boldsymbol{q} = x(1, 0, 0)2\pi/a$. The presence of the two-peak structure corresponding to the double branch in the spin-wave dispersion is clearly visible. The Gaussian broadening σ in equation (26) is 0.02 eV.

3.2. Ni(111)

Considering the cubic symmetry of Ni, one expects the spin-wave dispersion to be isotropic as confirmed by the experimental spectra. However, there is one puzzling feature in the spin-wave dispersion along the (111) direction: only one branch is observed, unlike in the (100) direction, and calculations by Savrasov [12] seem to confirm this. It is feasible that the double branch in the spin-wave dispersion is due to a complicated nesting structure of the Fermi surface which is sensitive to the direction in $\boldsymbol{k}$-space. On the other hand, the experimental resolution along the (111) direction is known to be worse than that along the (100) direction, so such a double-peak structure in the spin-wave spectra may be too fine to be observable [13]. It is therefore interesting to perform calculations to achieve a better understanding of this ambiguous feature. In numerical calculations, we can use an arbitrary 'resolution' by adjusting the broadening of the Gaussian. We have calculated the spin-wave dispersion along (111) using several different broadenings and the results are shown in figures 6 and 7. We adopt the same reduction in the exchange splitting as in the (100) direction. Using the same broadening as for the (100) direction we can clearly distinguish a prominent double peak in the spin-wave spectra. The results reveal that there is clearly an underlying double-peak structure which becomes smeared out when a larger broadening is used. The peak resulting from a larger broadening falls in between the two peaks corresponding to the smaller broadening. Therefore we have good reasons to believe that there also exist two branches along the (111) direction. The separation between the two peaks is actually so large ($\sim$70 meV) that it should not be too difficult to observe with better instruments whether the double-peak structure really exists.

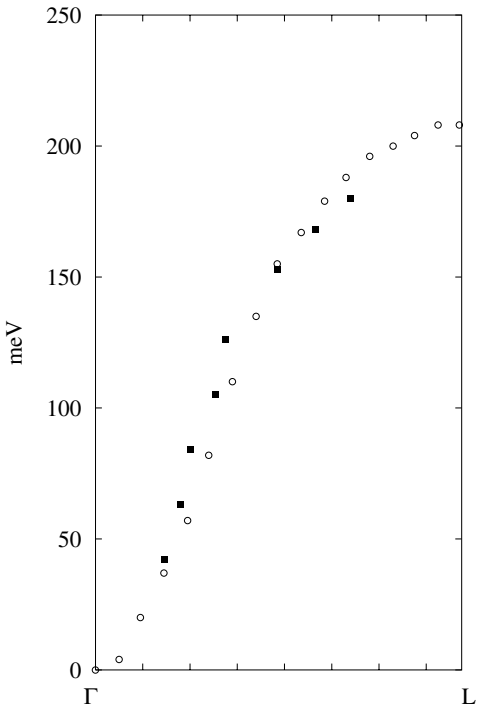

Figure 6. Spin-wave dispersion along (111) for nickel. Black boxes correspond to the experiment by Mook and Paul. The empty circles correspond to the present calculations with a Gaussian broadening σ in equation (26) equal to 0.08 eV.

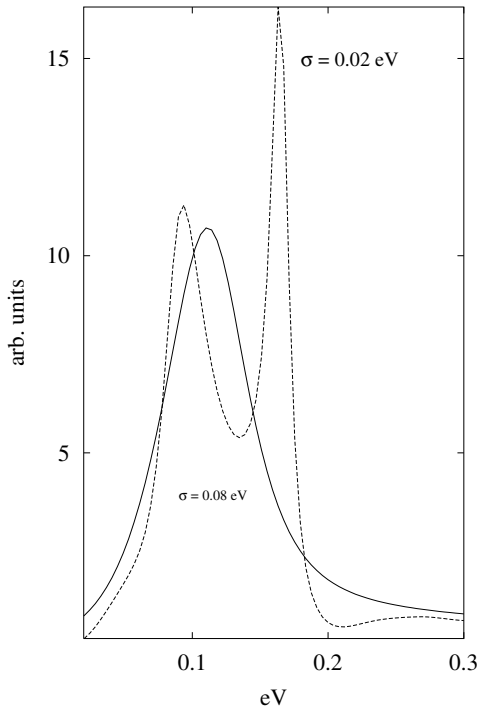

Figure 7. Spin-wave excitation spectra of nickel for $\boldsymbol{q} = 0.1875(1, 1, 1)2\pi/a$ for different broadenings.

3.3. Fe(110)

The experimental spin-wave dispersion of Fe does not appear to show anything peculiar [20,21]. Unlike for Ni, the dispersion only shows one branch. Previous calculations by Cooke *et al* [9] and Savrasov [12] are in agreement with this experimental result. One difference in the theoretical calculations is that Cooke *et al* found the dispersion to vanish towards the ZB whereas Savrasov found that the dispersion persisted to the ZB. In the Cooke *et al* calculations it was observed for $\boldsymbol{q} = 0.4(1, 0, 0)2\pi/a$ that the spin-wave linewidth increased dramatically, and in addition a high-energy optical spin-wave mode was found at ∼360 meV. In a more recent work by Blackman, Morgan, and Cooke [16], several branches were found persisting out to the ZB; however, the optical branch was too high in energy.

To further test our formalism, we also calculated the spin-wave dispersion and spectra of Fe. The LDA exchange splitting for Fe compares well with the experimental one (2.2 eV), so no reduction for the exchange splitting is introduced. Up to the available experimental data taken by Lynn [20], our results shown in figure 8 are in good agreement with experiment. In accordance with Savrasov [12], the spin-wave excitations persist out to the ZB, as indicated in figure 9. In fact, recent measurements [21] followed the spin-wave excitations to the ZB, and the observed energy at the ZB was ∼350 meV, in agreement with our predictions.

Within the experimental sensitivity there is no sign of two branches. But surprisingly, we found a gap in the spin-wave dispersion at $\boldsymbol{q} = 0.25(1, 1, 0)2\pi/a$ with a substantially lower energy than that of the optical mode found in [9, 16], as can be seen in figure 10.

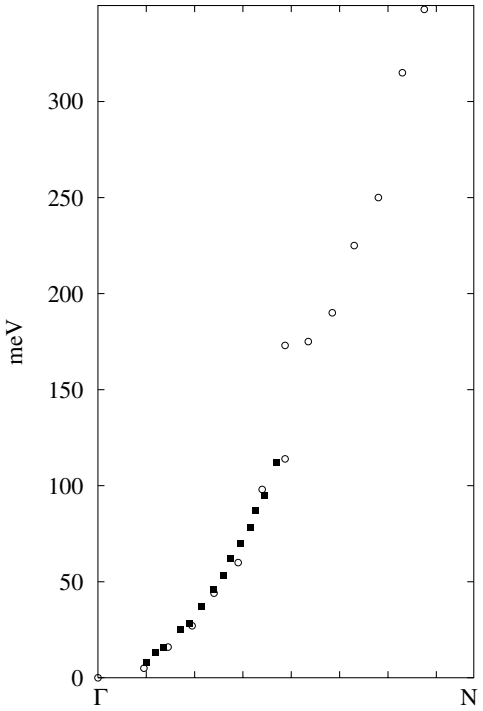

Figure 8. Spin-wave dispersion along (110) for iron. Black boxes correspond to the experiment by Lynn and the empty circles to the present calculations with a Gaussian broadening in equation (26) equal to 0.08 eV.

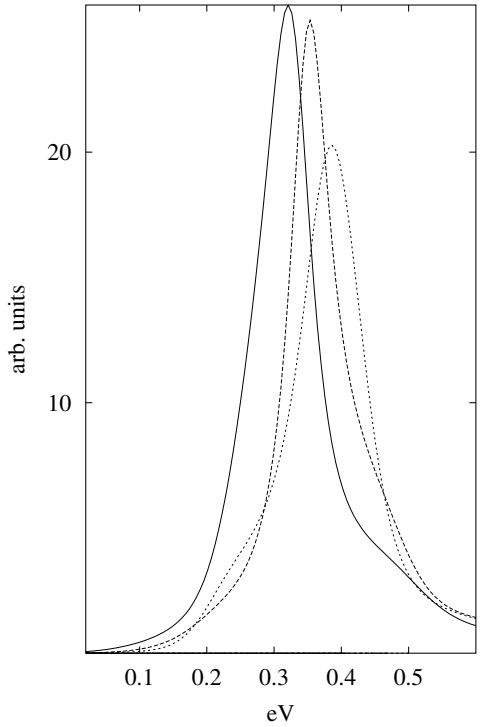

Figure 9. Spin-wave excitation spectra of iron for $\boldsymbol{q}$ close to the zone boundary. Decreasing spin-wave height corresponds to increasing $\boldsymbol{q}$, where $\boldsymbol{q} = x(1, 1, 0)2\pi/a$ with $x = 0.406\,25, 0.468\,75$ and 0.5, respectively.

A very interesting work on the temperature-dependent magnetization of Fe and Ni was recently published by Ododo and Anyakoha [22] where they analysed experimental data regarding the variation of magnetization with temperature. In order to explain the experimental magnetization curve, they concluded that there should exist a gap in the spin-wave dispersion at $\boldsymbol{q} = 0.25(1, 1, 0)2\pi/a$ and 170 meV, in perfect agreement with our findings. Considering that the double-peak structure in the calculated spectra shown in figure 10 is not as prominent as in the case of Ni, it is not surprising that such a structure may be difficult to observe experimentally. Our calculations and the analysis of Ododo and Anyakoha, however, give strong support for the presence of the gap in the dispersion. It is worth mentioning here that a spin-wave energy gap has also been found for some heavy rare-earth metals [30].

4. Concluding remarks

We have calculated the spin-wave spectra and dispersions in Ni and Fe using a newly developed Green's function formalism. In the present calculations, the simplest approximation equivalent to the RPA is used but the formalism is rather general and it allows for straightforward improvements beyond the RPA. The formalism treats localized and itinerant electrons on the same footing, unlike the frozen-magnon approach which makes an assumption about the localized nature of the spin. Since the magnetic response function is calculated explicitly, an arbitrary broadening can be used in the calculations which allows for a much smaller

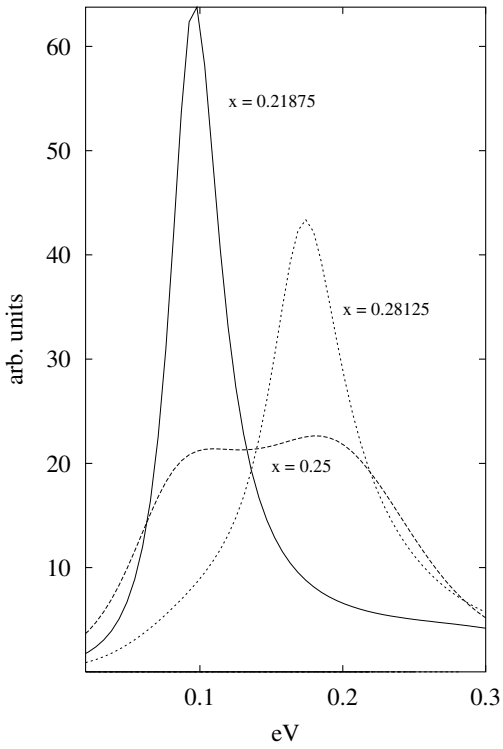

Figure 10. Spin-wave excitation spectra of iron for $\boldsymbol{q} = x(1, 1, 0)2\pi/a$.

'resolution' than the experimental one. This is in contrast to the Sternheimer approach used in TD DFT which requires a relatively large damping factor to achieve convergence.

We summarize below a number of findings from the present study:

- The calculated spin-wave dispersion of Ni(100) exhibits a double branch as also found experimentally and in previous calculations. Using the standard LDA band-structure the lower acoustic branch is found to be in good agreement with experiment but the energy of the optical branch is a factor of two too large compared with experiment. Reducing the exchange splitting by a factor of two leads to a much better agreement with experiment. Thus, it is reasonable to conclude that it is mainly the band-structure that determines the dispersion rather than the frequency dependence and nonlocality of $\mathcal{W}$.
- The acoustic branch of Ni(100) does not extend to the zone boundary as also confirmed experimentally.
- The calculated spin-wave dispersion of Ni(111) also shows a double branch which is not observed experimentally. The double branch is found only when a small broadening is used in the calculations. It is feasible that the experimental resolution is too low for observing the double branch.
- For Fe, a gap in the dispersion is found midway along Γ–N. This gap is not observed experimentally but an analysis of the temperature-dependent magnetization has predicted a similar gap at the same wave vector. Recent measurements on spin-wave dispersions in 4f systems have also found a similar gap. Consequently, we have good reasons to believe that such a gap actually exists.

It would be interesting to apply the present formalism to other ferromagnetic systems and to antiferromagnetic materials. Work along these lines is now in progress.

Acknowledgments

We gratefully acknowledge financial support from the New Energy and Industrial Technology Development Organization (FA) and the Swedish Natural Science Research Council (KK).

Appendix. Neutron cross section

The differential cross section for inelastic neutron scattering from a system of electrons is given by [31]

$$\frac{\mathrm{d}^2\sigma}{\mathrm{d}\Omega\,\mathrm{d}\omega} = \frac{1}{2\pi}\left(\frac{e^2 g}{mc^2}\right)^2 \frac{p_f}{p_i}\sum_{ij}(\delta_{ij} - e_i e_j)\int \mathrm{e}^{-\mathrm{i}\omega t}\langle S^i(\boldsymbol{q},0)S^j(-\boldsymbol{q},t)\rangle\,\mathrm{d}t \tag{A.1}$$

where $\boldsymbol{p}_i$ and $\boldsymbol{p}_f$ are the incident and scattered wave vectors, respectively, and $\boldsymbol{e} = \boldsymbol{q}/|\boldsymbol{q}|$ with $\boldsymbol{q} = \boldsymbol{p}_i - \boldsymbol{p}_f$. The neutron energy loss is $\omega = (p_i^2 - p_f^2)/2M$, m and M are the electron and neutron masses, respectively, and g is the neutron magnetic moment. Equation (A.1) takes into account the neutron–electron spin interaction only, since the interaction of a neutron and the translational (orbital) motion of the electrons in narrow energy bands are usually negligible. The spin operator $S^i(\boldsymbol{q},t)$ is given in the Heisenberg picture with

$$S^i(\boldsymbol{q},0) \equiv S^i(\boldsymbol{q}) = \int \mathrm{e}^{-\mathrm{i}\boldsymbol{q}\cdot\boldsymbol{r}}\Psi^\dagger(\boldsymbol{r})S^i\Psi(\boldsymbol{r})\,\mathrm{d}^3r \tag{A.2}$$

where $\Psi(\boldsymbol{r})$ is the two-component electron creation operator and $S^i = \frac{1}{2}\sigma^i$. The appropriate Green function to consider is defined by

$$\mathrm{i}G_{-+}(\boldsymbol{q},t) = \langle T[S^-(\boldsymbol{q},t)S^+(-\boldsymbol{q},0]\rangle \equiv G^>_{-+}(\boldsymbol{q},t)\theta(t) + G^<_{-+}(\boldsymbol{q},t)\theta(-t). \tag{A.3}$$

Using the invariance of the trace of a product of operators under their cyclic permutation, we note that

$$\begin{aligned}\frac{1}{2\pi}\int \mathrm{e}^{-\mathrm{i}\omega t}\langle S^i(\boldsymbol{q},0)S^j(-\boldsymbol{q},t)\rangle\,\mathrm{d}t &= \frac{1}{2\pi}\int \mathrm{e}^{-\mathrm{i}\omega t}\langle S^i(\boldsymbol{q},-t)S^j(-\boldsymbol{q},0)\rangle\,\mathrm{d}t \\ &= \frac{1}{2\pi}\int \mathrm{e}^{\mathrm{i}\omega t}\langle S^i(\boldsymbol{q},t)S^j(-\boldsymbol{q},0)\rangle\,\mathrm{d}t \equiv G^>_{ij}(\boldsymbol{q},\omega)\end{aligned} \tag{A.4}$$

By defining the spectral function $A_{ij}(\boldsymbol{q},t)$ as

$$A_{ij}(\boldsymbol{q},t) \equiv \langle S^i(\boldsymbol{q},t)S^j(-\boldsymbol{q},0) - S^j(-\boldsymbol{q},0)S^i(\boldsymbol{q},t)\rangle = G^>_{ij}(\boldsymbol{q},t) - G^<_{ij}(\boldsymbol{q},t) \tag{A.5}$$

we obtain

$$\begin{aligned}G^>_{ij}(\boldsymbol{q},\omega) &= [1+n(\omega)]A_{ij}(\boldsymbol{q},\omega) \\ G^<_{ij}(\boldsymbol{q},\omega) &= n(\omega)A_{ij}(\boldsymbol{q},\omega).\end{aligned} \tag{A.6}$$

Here we have used

$$G^>_{ij}(\boldsymbol{q},\omega) = \mathrm{e}^{\beta\omega}G^<_{ij}(\boldsymbol{q},\omega) \tag{A.7}$$

which is a consequence of the fact that

$$\langle S^i(\boldsymbol{q},t)S^j(-\boldsymbol{q},0)\rangle = \langle S^j(-\boldsymbol{q},0)S^i(\boldsymbol{q},t+\mathrm{i}\beta)\rangle \tag{A.8}$$

due to the invariance of the trace of a product of operators under their cyclic permutation. The occupation factor is given by

$$n(\omega) = (\mathrm{e}^{\beta\omega} - 1)^{-1}. \tag{A.9}$$

The spin-wave contribution to the total cross section is given by the $i = j = x$ and $i = j = y$ terms. We obtain then for the cross section

$$\frac{\mathrm{d}^2\sigma}{\mathrm{d}\Omega\,\mathrm{d}\omega} = \left(\frac{e^2 g}{mc^2}\right)^2 \frac{p_f}{p_i}\left[(1-e_x^2)G^{>}_{xx}(\boldsymbol{q},\omega) + (1-e_y^2)G^{>}_{yy}(\boldsymbol{q},\omega)\right]. \tag{A.10}$$

Using

$$S^{+}(\boldsymbol{q}) \equiv S^{x}(\boldsymbol{q}) + \mathrm{i}S^{y}(\boldsymbol{q}) \qquad S^{-}(\boldsymbol{q}) \equiv S^{x}(\boldsymbol{q}) - \mathrm{i}S^{y}(\boldsymbol{q}) \tag{A.11}$$

we find $G^{>}_{xx}(\boldsymbol{q},t) = G^{>}_{yy}(\boldsymbol{q},t)$ with

$$G^{>}_{xx}(\boldsymbol{q},t) = \frac{1}{4}\left[\langle S^{+}(\boldsymbol{q},t)S^{-}(-\boldsymbol{q},0)\rangle + \langle S^{-}(\boldsymbol{q},t)S^{+}(-\boldsymbol{q},0)\rangle\right] = \frac{1}{4}\left[G^{>}_{+-}(\boldsymbol{q},t) + G^{>}_{-+}(\boldsymbol{q},t)\right]. \tag{A.12}$$

We have assumed that $\langle S^{-}S^{-}\rangle = 0$ and $\langle S^{+}S^{+}\rangle = 0$. The cross section then reads

$$\begin{aligned}\frac{\mathrm{d}^2\sigma}{\mathrm{d}\Omega\,\mathrm{d}\omega} &= \frac{1}{4}\left(\frac{e^2 g}{mc^2}\right)^2 \frac{p_f}{p_i}(1+e_z^2)\left[G^{>}_{-+}(\boldsymbol{q},\omega) + G^{>}_{+-}(\boldsymbol{q},\omega)\right] \\ &= \frac{1}{4}\left(\frac{e^2 g}{mc^2}\right)^2 \frac{p_f}{p_i}(1+e_z^2)(1+n(\omega))\left[A_{-+}(\boldsymbol{q},\omega) + A_{+-}(\boldsymbol{q},\omega)\right].\end{aligned} \tag{A.13}$$

It is straightforward to show that $G^{>}_{+-}(\boldsymbol{q},\omega)$ and $G^{>}_{-+}(\boldsymbol{q},\omega)$ are real quantities. By using the identity

$$\int \langle DB(t)\rangle \mathrm{e}^{\mathrm{i}\omega t}\,\mathrm{d}t = \mathrm{e}^{-\beta\omega}\int \langle B(t)D\rangle \mathrm{e}^{\mathrm{i}\omega t}\,\mathrm{d}t \tag{A.14}$$

one can extract

$$G^{>}_{+-}(\boldsymbol{q},\omega) = \mathrm{e}^{\beta\omega}G^{>}_{-+}(-\boldsymbol{q},-\omega). \tag{A.15}$$

By using this relation one can easily show that equation (A.13) satisfies the condition of detailed balance:

$$\left[\frac{\mathrm{d}^2\sigma}{\mathrm{d}\Omega\,\mathrm{d}\omega}\right]_{\boldsymbol{q},\omega} = \mathrm{e}^{\beta\omega}\left[\frac{\mathrm{d}^2\sigma}{\mathrm{d}\Omega\,\mathrm{d}\omega}\right]_{-\boldsymbol{q},-\omega} \tag{A.16}$$

and the cross section reduces to

$$\begin{aligned}\frac{\mathrm{d}^2\sigma}{\mathrm{d}\Omega\,\mathrm{d}\omega} &= \frac{1}{4}\left(\frac{e^2 g}{mc^2}\right)^2 \frac{p_f}{p_i}(1+e_z^2)(1+n(\omega))\left[A_{-+}(\boldsymbol{q},\omega) - A_{-+}(-\boldsymbol{q},-\omega)\right] \\ &= \frac{1}{4}\left(\frac{e^2 g}{mc^2}\right)^2 \frac{p_f}{p_i}(1+e_z^2)\left[(1+n(\omega))A_{-+}(\boldsymbol{q},\omega) + n(-\omega)A_{-+}(-\boldsymbol{q},-\omega)\right].\end{aligned} \tag{A.17}$$

The information about the spin-wave excitations is contained in $A_{-+}(\boldsymbol{q},\omega)$. In fact, $A_{-+}(\boldsymbol{r},\boldsymbol{r}';\omega)$ is given in paper I (equation (104)), where we concluded that the spin-wave spectrum was given by peaks in $A_{-+}(\boldsymbol{q},\omega) \sim \mathrm{Im}\,\mathcal{R}_{-+}(\boldsymbol{q},\omega)$. Physically, $A_{-+}(\boldsymbol{q},\omega)$ corresponds to a process where the neutron loses energy ($\omega > 0$; magnon creation), and $A_{+-}(\boldsymbol{q},\omega) \sim \mathrm{Im}\,\mathcal{R}_{+-}(\boldsymbol{q},\omega)$ to a process where the neutron gains energy ($\omega < 0$; magnon annihilation). If we neglect the contribution arising from Stoner excitations, we have $A_{-+}(\boldsymbol{q},\omega) = \delta(\omega-\omega_q)$. In that case,

$$\frac{\mathrm{d}^2\sigma}{\mathrm{d}\Omega\,\mathrm{d}\omega} \sim \left[(1+n(\omega))\delta(\omega-\omega_q) + n(-\omega)\delta(\omega+\omega_q)\right] \tag{A.18}$$

where we have used $\omega_q = \omega_{-q}$. For low temperature, the magnon creation process clearly dominates because n is vanishing.

References

[1] Aryasetiawan F and Karlsson K 1999 *Phys. Rev.* B **60** 7419
[2] See e.g. Sandratskii L M and Kübler J 1992 *J. Phys.: Condens. Matter* **4** 6927
[3] Antropov V P, Katsnelson M I, Harmon B N, van Schilfgaarde M and Kusnezov D 1996 *Phys. Rev.* B **54** 1019
[4] Uhl M and Kübler J 1996 *Phys. Rev. Lett.* **77** 334
[5] Solovyev I and Terakura K 1998 *Phys. Rev.* B **58** 15 496
[6] Niu Q and Kleinman L 1998 *Phys. Rev. Lett.* **80** 2205
[7] Izuyama T, Kim D and Kubo R 1963 *J. Phys. Soc. Japan* **18** 1025
[8] Rajagopal A K 1978 *Phys. Rev.* B **17** 2980
[9] Cooke J F, Lynn J W and Davis H L 1980 *Phys. Rev.* B **21** 4118
[10] Callaway J, Chatterjee A K, Singhal S P and Ziegler A 1983 *Phys. Rev.* B **28** 3818
[11] Stenzel E and Winter H 1986 *J. Phys. F: Met. Phys.* **16** 1789
[12] Savrasov S Y 1998 *Phys. Rev. Lett.* **81** 2570
[13] Mook H A and Paul D McK 1985 *Phys. Rev. Lett.* **54** 227
[14] Cooke J F, Blackman J A and Morgan T 1985 *Phys. Rev. Lett.* **54** 718
[15] Aryasetiawan F 1992 *Phys. Rev.* B **46** 13 051
[16] Blackman J A, Morgan T and Cooke J F 1985 *Phys. Rev. Lett.* **55** 2814
[17] Brown R H, Nicholson D M C, Wang X and Schulthess T C 1999 *J. Appl. Phys.* **85** 4830
[18] Gebauer R and Baroni S 2000 *Phys. Rev.* B **61** 6459
[19] Bylander D M, Niu Q and Kleinman L 2000 *Phys. Rev.* B **61** R11 878
[20] Lynn J W 1975 *Phys. Rev.* B **11** 2624
[21] Boothroyd A T, Perring T G, Taylor A D, Paul D M^{c}K and Mook H A 1992 *J. Magn. Magn. Mater.* **104–107** 713
[22] Ododo J C and Anyakoha M W 1973 *J. Phys. F: Met. Phys.* **3** 2174
[23] Hedin L 1965 *Phys. Rev.* **139** A796
[24] Fetter A L and Walecka J D 1971 *Quantum Theory of Many-Particle Systems* (New York: McGraw-Hill)
[25] Aryasetiawan F and Gunnarsson O 1994 *Phys. Rev.* B **49** 16 214
[26] Andersen O K 1975 *Phys. Rev.* B **12** 3060
[27] Perdew J P *et al* 1996 *Phys. Rev. Lett.* **77** 3865
[28] Savrasov S Y 1999 private communication
[29] Springer M, Aryasetiawan F and Karlsson K 1998 *Phys. Rev. Lett.* **80** 2389
[30] Patterson C, McMorrow D F, Godfrin H, Clausen K N and Lebech B 1990 *J. Phys.: Condens. Matter* **2** 3421
[31] Marshall W and Lovesey S W 1971 *Theory of Thermal Neutron Scattering* (Oxford: Oxford University Press)